Int J Earth Sci (Geol Rundsch) (2008) 97:1057–1073
DOI 10.1007/s00531-007-0211-1

ORIGINAL PAPER

Salinization of groundwater in the North German Basin: results from conjoint investigation of major, trace element and multi-isotope distribution

P. Möller · S. M. Weise · M. Tesmer · P. Dulski · A. Pekdeger · U. Bayer · F. Magri

Received: 19 October 2006 / Accepted: 23 May 2007 / Published online: 12 July 2007

Abstract Conjoint consideration of distribution of major, rare earth elements (REE) and Y (combined to REY) and of H, O, C, S, Sr isotopes reveals that four types of groundwater are distinguishable by their chemical composition presented by spider patterns. REY patterns indicate thermosaline deep water and two types of shallow saline groundwaters. Presence of connate waters is not detectable. Sr isotope ratios distinguish three sources of Sr: fast and slow weathering of biotite and K-feldspar in Pleistocene sediments, respectively, and dissolution of limestones. δ^{13}C(DIC) indicate dissolution of limestone under closed and open system conditions. Numerous samples show δ^{13}C(DIC) > 13‰ which is probably caused by incongruent dissolution of calcite and dolomite. The brines from below 1,000 m represent mixtures of pre-Pleistocene seawater or its evaporation brines and infiltrated post-Pleistocene precipitation. The shallow waters represent mixtures of Pleistocene and Recent precipitation salinized by dissolution of evaporites or by mixing with ascending brines. The distribution of water types is independent on geologic units and lithologies. Even the Tertiary Rupelian aquiclude does not prevent salinization of the upper aquifer.

Keywords North German Basin · Salinization · Groundwater · Brine · Rare earth elements · H–C–O–S isotopes · Sr isotope ratio

P. Möller (✉) · P. Dulski · U. Bayer · F. Magri
GeoResearch Center Potsdam, 14743 Potsdam, Germany
e-mail: pemoe@gfz-potsdam.de

P. Dulski
e-mail: dulski@gfz-potsdam.de

U. Bayer
e-mail: bayer@gfz-potsdam.de

F. Magri
e-mail: Fabienma@gfz-potsdam.de

S. M. Weise
UFZ Helmholtz Centre for Environmental Research,
06120 Halle, Germany
e-mail: stephan.weise@ufz.de

M. Tesmer · A. Pekdeger
Free University Berlin, 12249 Berlin, Germany

M. Tesmer
Hanoi University of Science, Hanoi, Vietnam
e-mail: tesmer@zedat.fu-berlin.de

Introduction

Major and trace elements are subjected to different physico-chemical processes. Dissolution and alteration of major minerals establish the gross chemical composition of water, whereas trace elements are largely controlled by adsorption onto mineral surfaces, amorphous and colloidal matter and/or coprecipitation with alteration products. Nonetheless, the mineralogical composition of any catchment area constitutes the composition of the infiltrating water. The further development of groundwater composition depends on the types of rocks passed by the percolating water until reaching the ultimate aquifer. Mixing with residual formation (connate) water may also influence the composition. Human influences on water composition are not discussed herein.

Of particular interest in the North German Basin (NGB) are the upper aquifers at risk from ascending brines, especially as these aquifers are exploited by public services. In the North German Basin part of the groundwater resources cannot be used as drinking water because of natural salinization. Apart from coastal areas, where

infiltration of seawater occurs, groundwater salinization is mainly attributed to subrosion of salt diapirs and upconing of deep-seated brines. The origin of deep Ca–Cl brines as a water type, and particularly those in the Jordan-Dead Sea transform (Herut et al. 1990; Hardie 1990; Rosenthal 1997), have been discussed for many years (Lerman 1970; Starinsky 1974; Carpenter 1978; Frape and Fritz 1987; Spencer 1987; Nordstrom and Olsson 1987; Hanor 1994). The extreme views of salinization of groundwater are (1) mixing of evaporation brines and precipitation or seawater (Carpenter 1978) or (2) based on isotope data, dissolution of salts by precipitation only (Clayton et al. 1966). The high salt contents are explained either by dissolution of evaporites (Bennett and Hanor 1987; Bein and Dutton 1993) or by membrane effects (Graf et al. 1966; Kharaka and Berry 1973). Replacement of brines by fresh water is assumed to be not quantitative (Domenico and Robbins 1985; Knauth 1988). Most brines are altered in composition when taking part in processes such as dolomitization, albitization, ion exchange and precipitation of sulfates and carbonates. Saline water shows hydrostratigraphic layering (Bein and Dutton 1993; Mehta et al. 2000) with local deviations only near to diapirs.

In a recent paper analyses from oil exploration campaigns have been used to study the distribution of saline water in the NGB (Tesmer et al. 2007). These waters were collected from observation and production wells up to depths of 2,500 m. It turned out that the known aquicludes are not the barriers they were thought to be. Salinization is locally observed even at surface. In this contribution the groundwaters from different aquifer systems of the North German Basin are chemically and isotopically once more analysed in order to study the following topics:

- In which way do the underlying Zechstein salts influence the composition of the upper aquifers, which are exploited by public services?
- What kind of alteration processes is involved in changing the chemical composition of groundwater?
- Are formation (connate) waters still present and are they significantly involved in salinization process?
- To which depth can the influence of the Pleistocene exchange of water be traced?

Geological and hydrogeological settings

The North German Basin (NGB) is part of one of the world's largest evaporite containing sedimentary basins (Fig. 1). It is constraint by the Tornquist-Teisseyre Zone, to the south by the Elbe Line, and continues northwesterly into the North Sea and southeasterly into the Polish Basin. What makes this basin somewhat different from North American examples is the intensity of salt diapirism and the fact that glaciers covered the basin during the various stages of Pleistocene glaciations (Kloppmann et al. 2001). The intensive salt diapirism created salt pillows, walls and diapirs. Where salt diapirs reached the surface, they displaced the overlying sedimentary strata and generated topographic heights (Klinge et al. 1992). Southward-moving glaciers moulded today's morphology during the Weichsel glaciation period (corresponding to Wisconsin glaciation in North America) and formed the North German Plain with elevations of less than 100 m above sea level.

Hydrogeologically, the regional groundwater system can be divided into upper fresh water and several deep salt water systems (Fig. 2). The most important aquiclude with respect to groundwater management is the Lower Tertiary Rupelian Clay, which separates the Quaternary and Tertiary fresh water complex from the saline Mesozoic aquifer complexes (Lower Tertiary to Upper Triassic). In the Mesozoic strata (mainly carbonates, marls and sandstones), the groundwater salinization increases with depth, but is not restricted to stratigraphic units (Tesmer et al. 2007). The total dissolved solids (TDS) reach concentrations of 270 g/l at depth of around 2 km. Groundwater from Permian aquifer complexes (intra-saliniferous carbonates and fluvial sandstones) are near halite and anhydrite saturation. TDS in these groundwaters is rather uniform with mean values of about 300 g/l.

The fresh water complex consists of inhomogeneous Pleistocene sequences of gravel, sand, silt and clays, which are highly variable in thickness and lateral extension. Hydraulic connections between the fresh water body and the saline aquifer systems exist not only along fault zones but also along Pleistocene channels deeply cut into the underlying strata including the Rupelian Clay. In general, groundwater flow follows the regional slope of the North German Plain towards the Baltic Sea, (Zieschang 1974; Grube and Lotz 2004). Locally, the flow is directed from the topographic heights towards the receiving river systems. Artesian groundwater conditions are present in large morphological depressions.

In Fig. 1 three sites are specified. Morphologically dominant is the "Lübeck Basin" in the northern part of the NGB, which is a glacial basin with rim heights of about 80 m a.s.l. The study area is surrounded by several salt pillows (Eckhorst, Travemünde, Cismar) and the salt diapir of Bad Segeberg. An influence of salinized waters on drinking and industrial water production has been recognized for centuries (Grube and Lotz 2004). The main causes for shallow groundwater salinization are thought to be (1) dissolution of salt deposits (2) intrusion of seawater, and (3) up-coning of saline water (Tesmer et al. 2005).

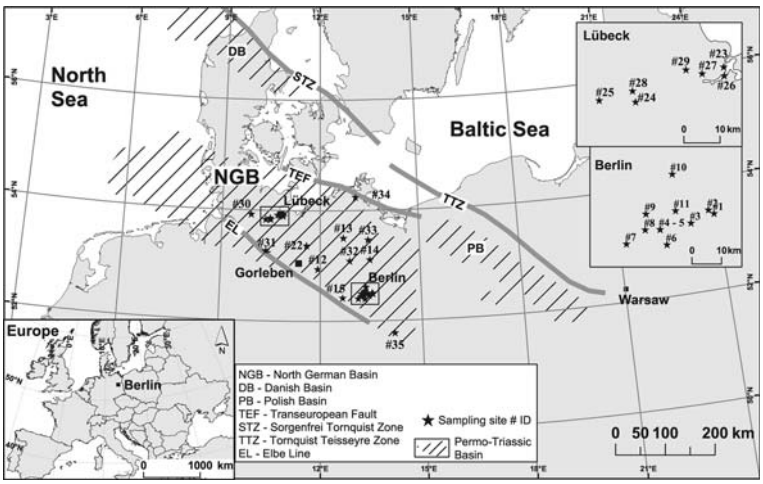

Fig. 1 Position of the North German Basin in Europe with sample localities. For information on sampling sites refer to Table 1

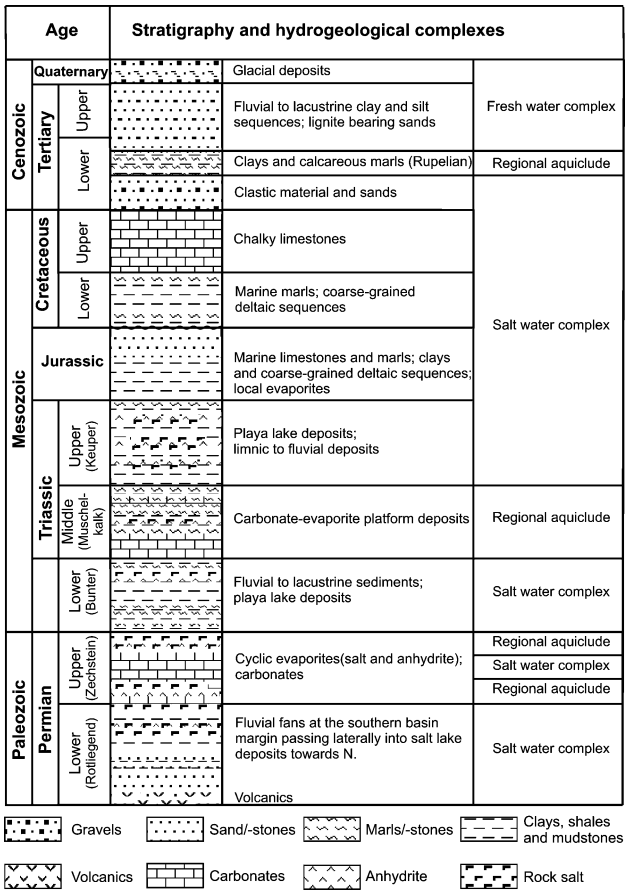

Fig. 2 Generalized columnar section of the stratigraphy and hydrogeological complexes of the North German Basin (modified after Scheck and Bayer 1999)

In the Berlin area, saline waters originating in deep-seated formations are encountered in Tertiary and Quaternary aquifers overlying the Rupelian Clay by cross-formational flow. Such interaquifer connections are prevalently due to erosion channels deeply cut into the Rupelian Clay and locally even reach the Upper Triassic strata. Discharge of brine into the shallow fresh water system mainly occurs in the southern part of the investigation area, where salt meadows and saline springs are known (Hannemann and Schirrmeister 1998; Grube et al. 2000).

The exploratory salt mine of Gorleben, which is intended for storage of high-level radioactive wastes, is one of the best studied areas in NGB. The salt structure of Gorleben salt dome is cut by a subglacial erosion channel. Tertiary clays and part of the cap-rock were eroded, so that the highly permeable channel fill is in contact with the Zechstein salt. As a result of the studies the predominant source of salinity (halite dissolution) is known, which allows to characterize isotopically a potentially "pure" mixing end-member (Buckau et al. 2000; Kloppmann et al. 2001; Berner et al. 2002).

Sampling and analytical procedures

All wells were pumped until electric conductivity, pH, temperature, and redox potential achieved steady state conditions. Water samples for anions, cations and REE, and isotope analyses were filtered on-line through 0.2 µm cellulose acetate filters (Sartobran®, Sartorius). Samples for cation analysis were preserved with concentrated nitric acid (HNO_3) at pH < 2. Alkalinity was determined by Gran titration immediately after sampling. Cations were measured by atomic absorption spectrometry (Perkin Elmer 5000) and anions were measured using ion chromatography (DX 100).

About 3 l of filtered water were spiked by Tm and acidified to pH 2 (low Ca contents) or pH 4 (if Ca > 0.1 mmol/l). Two to ten hours after pH adjustment the waters were passed through preconditioned Sep-Pak $C_{18}^{®}$ cartridges (Waters Corp. USA) that contain liquid cation exchanger. Later, the cartridges were washed and the REY were eluted with 40 ml

6 M sub-boiled HCl. After evaporation to dryness, the residues were taken up by 1 ml of 5 M sub-boiled HNO_3. These solutions were spiked by a Ru–Re mixture for possible corrections of the internal shift of the response factors in inductively coupled plasma mass spectrometry (ICP-MS) measurements if necessary (Bau and Dulski 1996) and filled up to 10 ml with purified water. Calibration solutions were prepared from single element standard solutions (CertiPUR® ICP standards Merck, Germany). Several corrections were necessary because of interferences of molecular ions with the desired mono-charged ions of the REE (Dulski 1994). Blank corrections for La, Ce, and Pr, which are contaminants of the commercially available liquid cation exchanger (Merck, Germany), were necessary. The efficiency as determined by either Tm single spike varies between 93 and 104%. Data are given by Tesmer et al. (2007).

For δ^2H and $\delta^{18}O$ determination, filtered water was purified by vacuum distillation as described in Knöller and Weise (in prep). A 0.5 µl of the distilled water were injected into a thermal combustion elemental analyzer (TC/EA; HEKATech) for pyrolysis at 1,400°C. The evolving oxygen immediately reacts with the carbon in the reactor tube to CO. H_2 and CO were separated in a gaschromatographic column and subsequently introduced via an open split (ConFlow II, Thermo Finnigan) into an isotope-ratio mass spectrometer (IRMS; Delta plus XL, Thermo Finnigan) for isotopic analysis. For matching with the common V-SMOW-SLAP scale, standard waters are integrated into a run of sample measurements (Vienna Standard Mean Ocean Water, V-SMOW). The external reproducibility is for δ^2H about 1.2‰ and for $\delta^{18}O$ about 0.2‰.

For determination of $\delta^{13}C$, $\delta^{34}S(SO_4)$, and $\delta^{18}O(SO_4)$ about 1.5 l of water were collected and made alkaline in order to retain CO_2 from degassing. $BaCl_2$ was added to precipitate $BaCO_3$ and $BaSO_4$. About 10 mg of dried and homogenized precipitate was filled into a vacutainer™, which was placed in a gasbench system (Thermo Finnigan), and flushed with helium. Warm phosphoric acid was added, and after about 2 h the released CO_2 was transferred via helium carrier into a Delta S IRMS. Sample analyses were bracketed by reference materials. Results of stable carbon isotope analyses are expressed in δ notation ($\delta^{13}C$) relative to V-PDB scale with an external reproducibility of 0.2‰.

From the remaining precipitate the carbonate was eliminated with 10 M HCl. After washing and drying the sample was split again. For $\delta^{34}S$ analyses the $BaSO_4$ was converted into SO_2 by use of an elemental analyzer (continuous flow flash combustion technique) coupled with an IRMS (Delta S, Thermo Finnigan). Sulfur isotope measurements were performed with a external reproducibility of ±0.3‰ and reported as ‰ variation relative to the Canon Diablo Troilite (CDT) standard (Yanagisawa and Sakai 1983). Oxygen isotope analysis on barium sulfate was carried out by high-temperature pyrolysis at 1,450°C in a TC/EA connected to a Delta plus XL IRMS (Thermo Finnigan) with an external reproducibility better than ±0.6‰. Results of oxygen isotope measurements are expressed in δ notation ($\delta^{18}O$) relative to V-SMOW (Knöller et al. 2006).

For the Sr isotope analysis, the filtered water samples were diluted with Rb–Sr double spike prior to conversion into chlorides with distilled 6 N HCl. After drying the samples, they were dissolved in 2.5 N HCl, and Sr was extracted by columnar elution using 5 ml quartz-glass columns filled with the cation resin Bio-Rad AG 50 W-X8, 200–400 mesh (Wiegand et al. 2001). The collected eluate was dried and finally dissolved in 1 µl of 0.25 N H_3PO_4 and loaded on Re-double filaments. The Sr-isotope compositions were measured at the with a Finnigan TRITON thermal ionization mass spectrometer. The values obtained for the NBS 987 interlaboratory reference material are 0.710252 ± 0.000006 (n = 20).

The results of chemical and isotope analyses are compiled in Table 1. Additionally, averages of water groups from Gorleben are collected from Kloppmann et al. (2001).

Data presentation

Spider diagrams

Based on the importance of Zechstein salts and the possible mixing of fresh water and saline marine formation water or marine evaporation brines, all groundwaters are normalized to modern seawater (Bruland and Lohan 2004). Normalized values of dissolved species El are indexed sw. Plotting Log El_{sw} has the advantage that (1) the number of log units is less than plotting the absolute data, (2) element relationships like those in seawater are recognizable by horizontal trends, and (3) dominantly dissolved minerals (halite, carbonates and sulfates) can be recognized by typical trends of their constituents. The grouping of species along the x-axis in Fig. 3 follows their chemical association: K, Na, Cl and Br represent the halide group (halite and sylvite). B, SO_4^{2-}, Ca, Sr, Mg, Ba, and HCO_3^- are constituents of the sulfate–carbonate group (Möller et al. 2006a). The pattern of marine brines at different evaporation stages, dissolved halite and complementary fractions of anhydrite and calcite for a fixed Ca value are displayed. All groundwaters with a significant contribution of seawater or marine evaporation brines are characterized by $K_{sw} \approx Mg_{sw}$, $B_{sw} \approx Br_{sw}$ because these are the solute species which are only precipitated towards the very end of the evaporation process. Trends such as $K_{sw} \approx Na_{sw} \approx Cl_{sw} \approx (r_{sw} \approx Mg_{sw}$ ($\approx SO_{4sw}$, if not chemically reduced)

Table 1 Compilation of chemical and isotope analyses of groundwaters from the North German Basin

ID #	Location	Stratigraphy	Depth (m)	TDS (mg/l)	pH	Temperature (°C)	Conductivity (μS/cm)	Na (mg/l)	K (mg/l)	Mg (mg/l)	Ca (mg/l)	Cl (mg/l)
1	Berlin, Köpenickerstr.	U Cret	222	789	8	12.9	866	158	7.4	14	40	63
2	Berlin, Alt Friedrichsfelde	U Cret	230	9,044	8	16.5	15,480	3,300	18.8	50	62	5,100
3	Berlin, Unstrutstr	Jur	278	27,689	7.2	15.2	41,800	9,600	44.6	220	350	15,900
4	Berlin, Fabeckstr. (deep)	U Tert	203	2,399	7.1	11.5	3,890	790	6.1	7.8	21	1,025
5	Berlin, Fabeckstr. (shallow)	Quart	88	494	7.1	11.03	557	50	2.2	8	64	7
6	Berlin, Osdorferstr.	L Tert	281	23,454	7	11.2	37,800	8,500	40	120	160	13,540
7	Berlin, HMI	U Trias	127	8,087	7.7	15.1	12,580	2,500	20.5	70	200	3,100
8	Berlin, Fischerhüttenw.	U Tert	169	5,088	7.8	10.07	8,670	1,680	11	26	80	2,610
9	Berlin, Postfenn	U Trias	218	45,858	7.3	15.9	64,000	14,700	68	360	1,260	24,500
10	Berlin, Lübars	Jur	185	17,708	7.7	15.2	30,200	6,200	36	128	160	10,600
11	Berlin, Reichstag	Jur	300	29,591	6.9	59.3	42,500	10,400	52	250	300	18,000
12	Bad Wilsnack	U Trias	1,000	160,126	6.1	19.3	184,600	57,200	320	1,050	2,400	97,790
13	Waren	U Trias	1,500	155,337	5.6	58	168,000	54,900	190	860	2,700	95,408
14	Templin	Jur	1,616	163,098	5.8	21.2	1,800	58,500	290	1,100	2,200	98,130
15	Belzig	U Trias	773	191,275	6.1	21.7	195,200	71,000	375	1,100	1,400	113,294
22	Neustadt Glewe	U Trias	2,250	218,698	5.1	77.4	218,000	70,900	760	1,450	9,000	135,550
23	Dummersdorfer Ufer	U Tert	105	4,699	7.2	10.8	7,960	1,350	34	95	202	2,300
24	Reinfeld	U Tert	210	8,893	7.4	10.7	15,680	3,180	40	48.5	100	4,960
25	Travenbrück	U Tert	250	42,993	7.3	13.2	64,000	15,700	129	176	760	24,700
26	Kleine Holzwiek	Quart	196	4,541	7.7	11.5	7,470	1,535	18	51.5	75	2,350
27	Am Brook	U Tert	86	1,787	7.1	10.5	2,700	284	8	30	255	670
28	Vosskaten	U Tert	299	12,535	7.6	10.6	20,700	4,630	46	67	92	6,920
29	Bad Schwartau	L Tert	300	36,057	7	16.3	54,200	11,800	100	625	960	22,200
30	Bad Bramstedt	U Perm	246	273,480	6.6	17.8	231,000	106,000	210	230	1,700	160,000
31	Lüneburg	U Perm	50	28,5522	6.6	16.8	233,000	102,500	3,750	2,700	700	167,000
32	Rheinsberg	U Trias	1,600	147,255	6.6	16.6	183,400	55,100	375	940	2,380	85,400
33	Neubrandenburg	U Trias	1,300	142,434	6.3	44.9	148,800	50,800	184	690	2,250	87,300
34	Mesekenhagen	U Perm	2,000	308,542				97,000	2,950	6,500	11,600	190,000
35	Burg	L Trias	1,300	244,330	6.7	20	211,000	87,000	690	820	3,800	150,000
Averages of Grorleben groundwaters (gw) and brines after Kloppmann et al. (2001)												
	Fresh gw		4–90	473	7.2			23.3	4.15	11.5	85.8	40.5
	Brackish gw		4–106	2667	7.4			664	6.73	39.3	237.7	1,456
	Saline gw		70–230	65,500	7.3			12,600	239	490	1,158	37,850
	Brines		140–236	317,000	7.0			121,333	1,303	1,280	1,263	185,670

Table 1 continued

SO_4(mg/l)	HCO_3 (mg/l)	Br (mg/l)	Sr (mg/l)	Ba (mg/l)	$\delta^{18}O$ (‰)	δ^{2} (H‰)	$^{34}S(SO_4)$ (‰)	$\delta^{18}O$ (SO_4) (‰)	$\delta^{13}C$ (DIC) (‰)	$^{87}Sr/^{86}Sr$	REY type	Spider type
3	503	0.4	0.8	0.1	–8.73	–61.6	16.9	1.8	–13.6	0.708551	R2	S2a
19	494	3	3.5	1.5	–9.41	–66.0	3.8	6.6	–3.67	0.707818	R1	S1a
1,300	275	12.3	13	0	–9.01	–59.7	21.3	18.5	–17.6	0.708338	R1	S2a
70	479	0.3	0.3	0	–9.34	–67.8	40.9	16	–13.7	0.708585	R2	S1a
3	360	0.2	0.3	0.1	–9.04	–64.1	13	5.6	–13.3	0.709496	R1	S2a
550	544	8.2	5.5	0.1	–8.92	–61.0	37.3	18.8	–15.5	0.708241	R1	S1a
2,000	197	2.4	8		–10.6	–75.9	19.8	17.9	–16	0.708342	R2	S1a
175	506	2.2	1.1	0	–9.85	–72.1	40.2	16.5	–13.2	0.708581	R1	S1a
4,500	470	55	28	0	–7.3	–49.4	22	16.3	–22.7	0.708260	R2	S1b
200	384	11.4	11	0.1	–8.52	–57.3	51.5	15.8	–15.4	0.708056	R1	S1a
308	281	18.8	21	0.1	–8.5	–56.0	48.2	20.2			R2	S1a
1,200	165	122	100	0.3	–3.42	–20.1	26.6	14.9	–14.6	0.708701	R3	S1a
1,150	128	117	130	0.5	–3.25	–21.2	26.2	17.2	–13.8	0.709189	R3	S1a
2,700	177	129	85	0.2	–3.97	–24.3	23.2	15.8	–13.5	0.708569	R3	S1a
3,840	265	64.8	40		–7.44	–42.5	20.4	13.6	–18.9	0.708465	R2	S1b
900	137	133	450	4.4	–1.45	–17.9	15.1	9.2	–11	0.710576	R3	S1a
300	418	8	3.1	0.1	–7.22	–51.4	20	12.3	–12.5	0.708520	R2	S3
122	442	0.75	2.8	0.1	–8.65	–60.1	29.5	18	–14.7	0.707970	R2	S1b
1,060	468	6.3	7.4	0.1	–9.37	–64.3				0.707985	R1	S1a
11	500	0.39	4.5	2.9	–8.66	–62.3	11.3	15.6	–8.2	0.707875	R2	S1a
45	494	2	1.2	0.2	–8.05	–56.2	30.3	15.7	–13.7	0.709290	R2	S3
205	540	3	1.5	0	–9.46	–67.2	24.7	20.6	–14	0.708430	R2	S1b
65	307	40	78	0.5	–6.1	–45.7	11	16.6	–11.1	0.707765	R1	S1a
5,200	140	19	23	0	–9.9	–66.8	11.3	–3.2	–10.8	0.707650	R2	S1b
8,600	271	114	7.9		–8.2	–45.7	10.9	13.6	–12.4	0.707745	R1	S4
2,740	320	107	74	0.3	–4.3	–30.4	26.1	16.8	–12.8	0.708499	R3	S1a
1,000	210	90	100	0.4	–4.1	–29.3	32.1	20.5	–12.9	0.708677	R3	S1a
370	122	1,290	580	1	4.0	–14.4					R2	S1a
1,630	390	300	98	0.2	–4.0	–27.3					R3	S1b
51	228	0.06	0.4		–8.55	–60.2				0.7094		
293	203	0.45	1.46		–8.77	–60.5				0.7100		
2,508	227	20	19		–9.9	–70.2				0.7080		
5,817	146	60.7	24		–8.8	–60.1				0.7076		

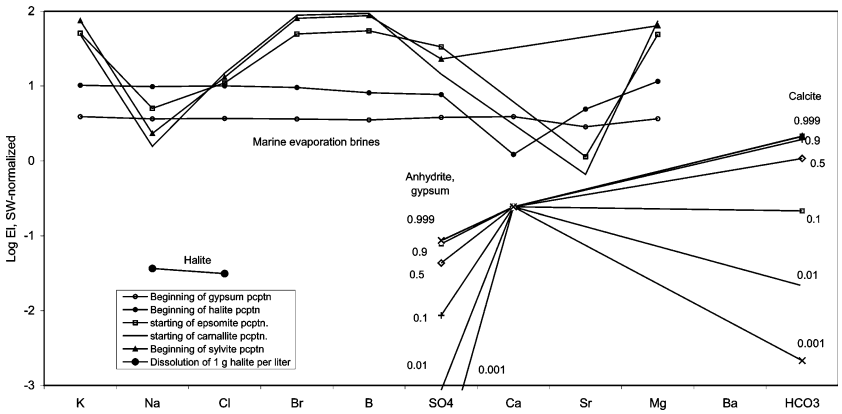

Fig. 3 Spider pattern of marine evaporation brines (after Fontes and Matray 1993). In addition the patterns of dissolved halite (1 g/l) and anhydrite/calcite mixtures (fractions are given by assigned figures) based on 0.1 g of Ca^{2+} dissolved in 1 l are shown

indicate the presence of seawater (connate water or intrusion of seawater). Residual amounts of marine evaporation brines may be overprinted by mixing with brines from various sources or by interaction with wall rock minerals, e.g., during dolomitization or albitization. Indicative segments are the following ones: Na_{sw}–Cl_{sw}–Br_{sw} typifies the dissolution of either halite or post-halite evaporites; B_{sw}–SO_{4sw} is largely controlled by anhydrite which is enriched in B by coprecipitation (Farber et al. 2004; Möller et al. 2007); Ca_{sw}–Sr_{sw} discriminates late diagenetic calcite from early diagenetic calcite, aragonite and anhydrite (Möller et al. 2006a) because in the course of diagenesis calcite looses Sr (Bausch 1968). $HCO_{3sw} > Ca_{sw}$ indicates dominant dissolution of carbonates, whereas $Ca_{sw} > HCO_{3sw}$ reveals dominance of anhydrite dissolution. $Ca_{sw} \approx HCO_{3w}$ reveals 10% carbonate and 90% anhydrite dissolution. Anhydrite dissolution is paralleled by enhanced contents of B_{sw} and SO_{4sw} if not reduced to H_2S (Möller et al. 2007).

Thus, spider patterns are a tool to characterize the chemical evolution of groundwaters. Changes of normalized concentrations depend on the presence of soluble minerals, which characterize the source of solutes (high salinity) but not the source of water.

REY distribution patterns

Among the trace elements, the series of REY are of particular interest because they are omnipresent in minerals and show characteristic distribution in minerals. REY/Ca weight ratios in minerals such as calcite and anhydrite are higher by about a factor of hundred than in groundwater. Therefore, REY are strongly adsorbed onto surfaces and coatings of minerals. Long before water is saturated with respect to calcite, it is already saturated with respect to REY. Thus, precipitation is saturated with REY, when it comes into contact with sediments, soils or rocks of the recharge area. Further dissolution of any mineral cannot alter REY composition as long as the lithology does not change. In case of change, it is important what kind of new minerals dissolves or undergoes alteration. Dissolution of minerals may release REY at concentration levels exceeding those in water. Most of the released REY are immediately adsorbed onto mineral surfaces without influencing the bulk of the water significantly (Möller et al. 2007). In case of alteration reaction in which large quantities of water are involved, mixing of the REY from dissolving minerals and those in water occurs. Such processes could be dolomitization of limestones or albitization of mafic igneous rocks (Möller et al. 2007). Therefore, REY patterns indicate either the dominantly soluble minerals in the catchment or alteration reactions of bulk rocks along the flow path. Dissolution of halite does not affect REY because their REY level is at the verge of the limit of detection. Dissolution of anhydrite has some effect on the final composition because the sulfates are more soluble than the carbonates.

A second thought should be given to mineral surfaces along the flow path of water. Neglecting any induction period in newly fractured rocks, these surfaces behave like an ion exchanger loaded with REY after the breakthrough of REY. From this time onwards REY patterns in aquifers resemble those established in the catchment. This can also be the case if the lithology changes but does not contain minerals of high solubility and bulk mineral alteration reactions (e.g., dolomitization, albitization, chloritization) are minor. Even if these waters pass different lithologies, the effect on REY distribution is negligible because all newly released REY have to be adsorbed. Adsorption takes place directly at the surface of the dissolving minerals and mostly within pores. This explains why REY patterns indicate the lithology of the catchment and why REY patterns are a reliable tool in grouping waters of seemingly the same origin.

Conventionally, REY abundances are presented as normalized distribution patterns. Here, normalization with C1 chondrite (Anders and Grevesse 1989) is preferred because its REY abundance is least fractionated. In

contrast, normalization to shale composites such as PAAS and NASC (McLennan 1989) alters Eu anomalies by increasing positive and decreasing negative ones because shales show small negative Eu anomalies with respect to C1 chondrite.

Variations in isotope composition

Data of stable isotopes of light elements (up to sulfur) are commonly given in the δ notation. Sr isotopes are given by their ratio. The water isotopes (H and O) can validate the flow path predicted by hydrogeological consideration. Solute isotopes collected along the flow path provide information about the sources of minerals that are contributing to the composition of water. In general, carbonates and plagioclase contain the least radiogenic Sr, whereas K-feldspars and micas contain the most radiogenic Sr reactive minerals (Bullen and Kendall 1998). $\delta^{13}C$ provides unique information on the origin of carbonate alkalinity and the relative importance of processes such as carbonate mineral dissolution, silicate hydrolysis, oxidation of organic matter and methanogenesis (Mills 1988; Katz et al. 1995). $\delta^{34}S(SO_4)$ reveals the sources of sulfates and the processes in which sulfur is involved such as bacterial activity.

Results

Major and minor element distribution

The spider patterns allows visual grouping of water samples according to specific features of the patterns. The following groups S1 to S4 emerge in NGB:

Type S1: The segment K_{sw}–Na_{sw}–Cl_{sw}–Br_{sw} in Fig. 4a displays the dissolution of halite as the main source of Na, Cl and Br. Additional Na may also originate from cation exchange with clay minerals or from weathering of albite. The low K_{sw} and Br_{sw} values prove the absence of sylvite in leached evaporites. Only #34 shows the presence of sylvinite by enhanced K_{sw} and Br_{sw}. The S1 type is divided into two subgroups because of different trends in SO_{4sw}–Ca_{sw}–Sr_{sw}–HCO_{3sw} and B_{sw}–SO_{4sw}:

- S1a: $Ca_{sw} < Sr_{sw}$ and—in many cases—$B_{sw} \approx Na_{sw}$ indicates dominant dissolution of anhydrite and probable mixing with Ca–Cl brine (Fig. 4a, b); $B_{sw} \geq SO_{4sw}$ point to strong sulfate reduction (Fig. 4a) which is less in Fig. 4b;
- S1b: $Ca_{sw} \leq HCO_{3sw}$, $Ca_{sw} \leq Sr_{sw}$ and $B_{sw} \leq SO_{4sw}$ suggest less sulfate reduction than in type S1a (Fig. 4c). The Gorleben Na–Cl brines resemble type S1b.

Type S2 shows a different trend. Halite dissolution is much less than in type S1 waters and carbonate dissolution dominates (Fig. 5a). $Na_{sw} >> Cl_{sw}$, and $Ca_{sw} << HCO_{3sw}$ may indicate cation exchange of Ca against Na on clay minerals. $K_{sw} > Br_{sw} > Cl_{sw}$ indicate dissolution of sylvite, which may go together with high B_{sw} indicating mixing with post-halite brines. Anhydrite dissolution is negligible.

Type S3 is characterized by $K_{sw} \approx Na_{sw} \approx Cl_{sw} \approx Br_{sw} \approx B_{sw} \approx SO_{4sw}$ trend which indicates mixing of fresh water and seawater, and $Ca_{sw} > Na_{sw}$ proves subsequent dissolution of carbonates (Fig. 5b).

Type S4 shows high $K_{sw} \approx Na_{sw} \approx Cl_{sw}$ dominating all the others. $HCO_{3sw} < Cl_{sw}$ but $Cl_{sw} > Br_{sw}$ indicate dissolution of halite and sylvite together with minor anhydrite and very little carbonate (Fig. 5b).

REY distribution

C1-chondrite-normalized REY patterns are grouped according to their trends (Fig. 6). Three different types emerge:

Type R1: Concave-shaped patterns (Fig. 6a) are controlled by oxygen-rich waters due to the precipitation of FeOOH during the weathering of Fe(II)-bearing minerals (Bau 1999; Kawabe et al. 1999; Quinn et al. 2004). In any case, these waters represent interaction with Quaternary sediments.

Type R2: Patterns of this group decrease from La to Eu and flatten thereafter (Fig. 6b). This type of patterns is typical for middle to late diagenetic limestones, geologically speaking Cretaceous and older (Möller et al. 2003). Water–rock interaction with limestone involves dissolution of calcite. Therefore, water and limestones have the same type of pattern. R2 is typical for water derived from Cretaceous to Triassic limestones in the study area.

Type R3: Patterns decreasing from middle to heavy REY (Fig. 6c) are typical for waters that experienced enhanced temperatures in water–rock interaction, i.e., for waters from depths below 1,000 m (Möller et al. 2003, 2006b).

Considering the source of all samples as given in Table 1 the S and R types are in no way related to geological formations and their specific rock compositions, which means that the chemical composition is hardly relatable to the source of saline waters.

In the Piper diagram (Fig. 7) the water samples are given by their R type signatures. The various R types either cluster or scatter widely. R1 type of water represents Na–Cl type of saline water with only one exception, which has been turned into Ca–HCO_3 type of water due to interaction with limestones. R2 types scatter widely. Type R3 represents Na–Cl brines, which plot together with type R1 saline

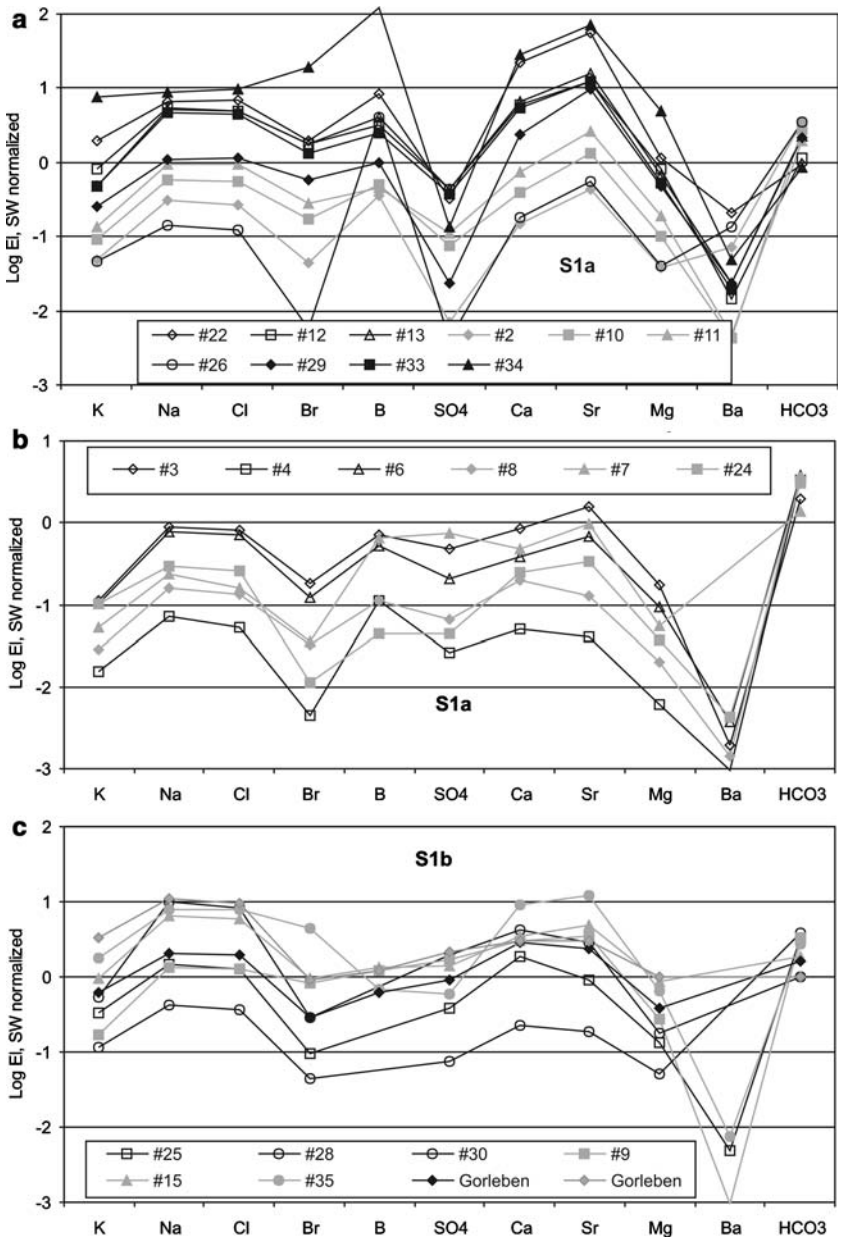

Fig. 4 Spider patterns of S1 type of saline groundwaters: **a** dominated by dissolution of halite and anhydrite and mixing with Ca–Cl brine, dissolution of limestone is minor; **b**, **c** dominated by dissolution of anhydrite and limestone in varying proportions

waters. Using REY characterization structures the distribution of samples in the Piper diagram.

Water isotopes

In Fig. 8, most of δ^2H and δ^{18}O plot along the global meteoric water line (GMWL; Craig 1961). Mean isotope composition of modern groundwater in northern Germany shows δ^2H values of –60‰ and (δ^{18}O values of –8‰ (Table 1). The range of our measurements corresponds to that reported by Kloppmann et al. (2001) on Gorleben saline waters. Compared with modern precipitation (in Berlin: δ^2H: –55.0‰; δ^{18}O: –7.70‰) most waters indicate lower average temperatures than today. Any mixtures of recent precipitation and Pleistocene precipitation or melt water from the ice shield overlays the global MWL. Most of the isotopically heavy, deep brines (type R3) plot on a mixing line of meteoric and seawater (represented by SMOW) or its evaporation brines both of pre-Tertiary age. The shift of two samples to higher δ^{18}O values may be due to hydrothermal isotope exchange (Giggenbach 1992; Clark and Fritz 1997) or mixing with extreme marine evaporation brines (Sofer and Gat 1972).

Sr isotope ratio versus 1/Sr

Clastic debris of granites and metamorphic rocks from the Scandinavian shield cover NGB up to several 100 m. They

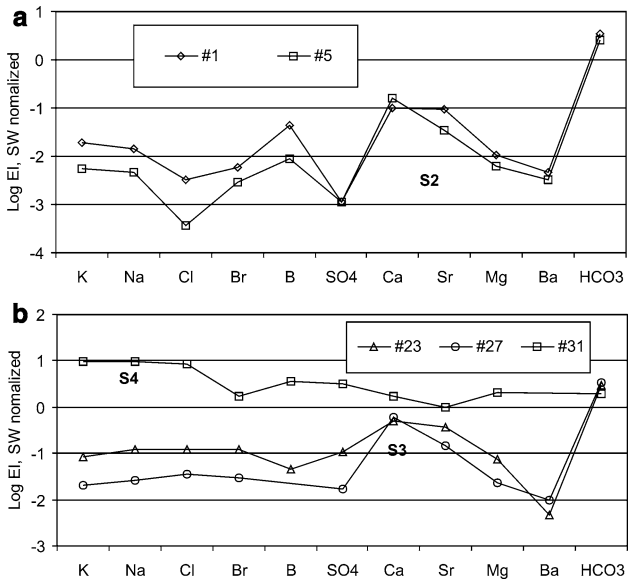

Fig. 5 Spider patterns of S2, S3 and S4 type of groundwaters: **a** water controlled by limestone dissolution (S2 type); **b** mixing of both infiltrating precipitation and seawater (type S3), and dissolution of a halite body by infiltrating precipitation (S4 type)

are composed today of mostly quartz, little K-feldspar and clay minerals. Originally, it may have contained also biotite, which degraded to hydrobiotite and clay minerals with time. Thus, two important Sr sources can be assumed: Biotite with both high Rb and Sr, and K-feldspar with low Sr but enough Rb in order to increase $^{87}Sr/^{86}Sr$ ratios by radioactive decay of ^{87}Rb. Blum and Erel (1995) suggested that deglaciation may enhance initial weathering of biotite relative to feldspar, but that the rate of biotite weathering slows down with time and most of the radiogenic Sr is lost to the melt water. Weathering of the more stable K-feldspar yields low Sr solutions and may represent a much later process. Thus, an early and a late weathering solution interact with Permian to Cretaceous limestones and Tertiary marls (Fig. 9).

The interaction of melt water with pre-Cretaceous limestones yields the trend of the thermo-mineral waters (type R3). More recent precipitation leaches Sr from K-feldspar and these shallow waters of type R1, which locally interact with marls and limestones during infiltration (type R2). These shallow groundwaters may be salinized by relics of brines or locally by ascending brines.

Thus, Sr isotopes yield insight into cycling of Ca as one of the most important elements in saline solutions. At closer look, the samples of type R1 and R2 in Fig. 9 can be split into three entities each of which is characterized by a range of Sr isotope ratio: (1) ratios of about 0.7094 assemble water from depths less than 100 m, i.e., interaction with youngest carbonates only; this group also includes averages of brackish and fresh water samples from Gorleben; (2) ratios between 0.7086 and 0.7082 of mostly R2 type may be controlled by Tertiary marls, and (3) ratios between 0.7080 and 0.7076 (fully in the range of Cretaceous to Upper Permian limestones) with R1 and R2 types of waters which also includes an average of saline waters and brines from Gorleben. The latter two groups are typical for waters that interacted with limestones or carbonate-rich boulder clay. The different nearly horizontal trend lines may indicate interaction with limestones of variable Sr contents.

Sulfur and oxygen isotopes in sulfate

$\delta^{34}S(SO_4)$ versus $\delta^{18}O(SO_4)$ (Fig. 10a) show two trends. Some correlation seems to exist in the range of low isotopic values. For $\delta^{34}S(SO_4) > 20‰$, $\delta^{18}O(SO_4)$ is virtually constant. Fields of Upper Permian and Triassic/Jurassic sulfates (Claypool et al. 1980) show that only brine #22 plots near to the average of Zechstein sulfates at Gorleben (Berner et al. 2002). Values of $\delta^{34}S(SO_4)$ exceeding 30‰ indicate bacterial reduction of dissolved sulfate due to which the heavier species remain in solution. Sample #2, either experienced oxidation of H_2S derived from chemical reduction of precursor sulfates or represents oxidation of igneous sulfides.

The scatter plot (Fig. 10a) shows that R1 and R2 type of waters cover the whole field, whereas the deep brines of type R3 water cluster in the middle. This result shows that mixing of sulfate from various sources and/or oxygen isotope exchange played a major role in the NGB.

The shallow samples #1, #2, and #5 with both low $\delta^{18}O(SO_4^{2-})$ and sulfate concentrations (Table 1) could represent atmospheric input (Berner et al. 2002). This source, however, cannot account for sample #30 with its high sulfate concentrations of 5,200 mg/l. With the rate of oxygen isotope exchange in the sulfate–water system being very slow at low temperatures, other processes have to be considered. The samples #1, #2, #5, and #30 originate from shallow depths and their trend may indicate sulfate–water O-exchange along with enzymatic processes during sulfate reduction (Fritz et al. 1989; Toran and Harris 1989; Van Stempvoort and Krouse 1994). In Fig. 10b the oxygen fractionation between sulfate and water is checked. Different from Berner et al. (2002) samples in this study show a wide range of $\Delta^{18}O = \delta^{18}O(SO_4) - \delta^{18}O(H_2O)$. $\Delta^{18}O$ value of about 28‰ roughly corresponds to sulfate–water O-isotope equilibrium at about 15°C (Berner et al. 2002).

The Upper Permian to Middle Triassic anhydrite was and probably still is dissolved by at least two isotopically different groundwaters (Fig. 8): mixtures of precipitation

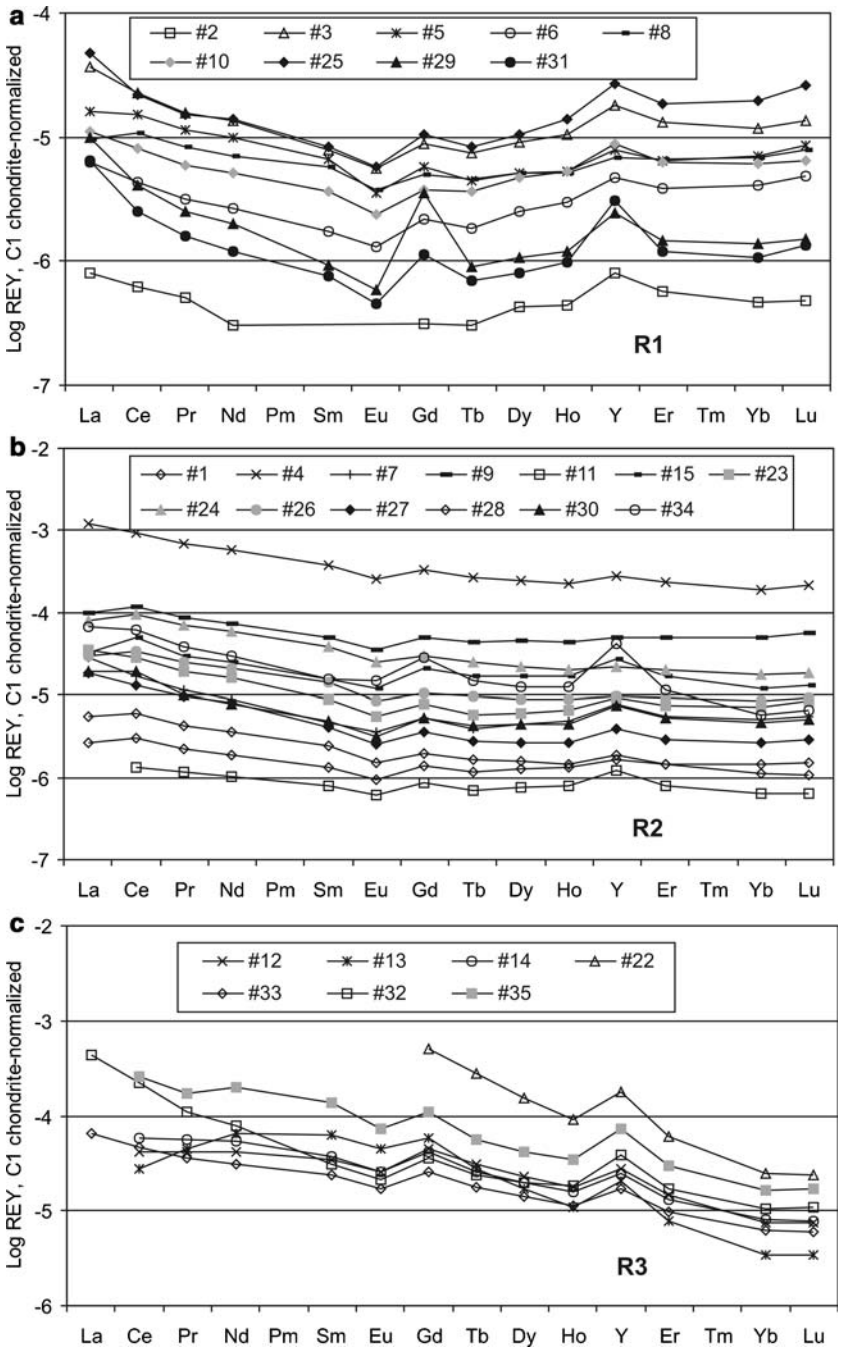

Fig. 6 Rare earth and Y distribution patterns in R1, R2, and R3 type of groundwaters. **a** Weathering solutions of Pleistocene sediments and soils; **b** dissolution of limestones; **c** thermo-saline deep groundwater

and seawater or its evaporations brines (type R3), which yield isotopically heavy water now residing at depths below 1,000 m as thermo-mineral brines, and isotopically light mixtures of Pleistocene and Recent precipitation occupying the aquifers at lower depths.

In both $\delta^{34}S(SO_4)$ and $\delta^{18}O(SO_4)$ versus SO_4/Cl (Fig. 11) typical sources of water can be outlined (Berner et al. 2002). Figure 11a elucidates that few samples still show Upper Permian $\delta^{34}S(SO_4)$ (like Gorleben) but most of them plot between the array of bacterial sulfate reduction and the Upper Permian salts. Again type R1 and R2 waters cover the whole field, whereas R3 type of waters cluster in the field of mixing. In the $\delta^{18}O(SO_4)$ plot only #22 in the field of true Permian signature and all other type R3 samples plot in the field of salinized shallow groundwaters (Fig. 11b). The shallow Sample #5 is the only one being characteristic for the meteoric sulfate pool.

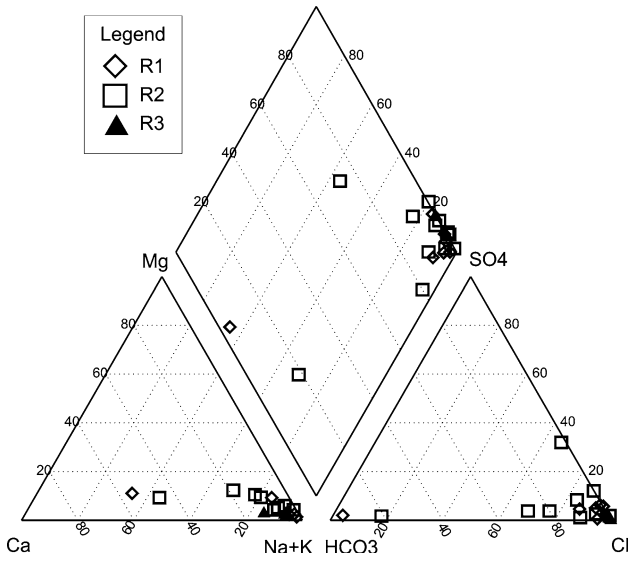

Fig. 7 Piper diagram. The water samples are presented according to their R type signature

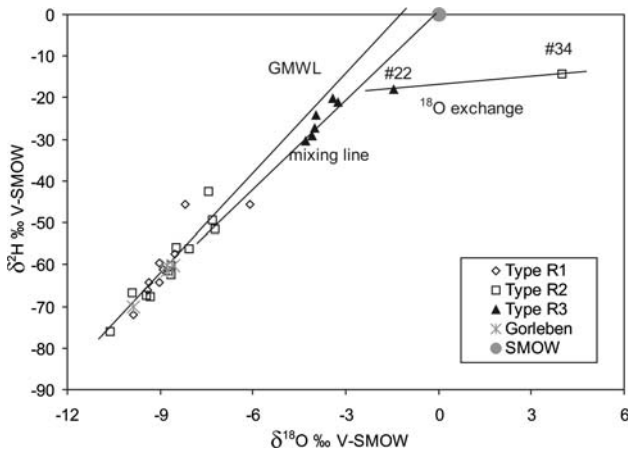

Fig. 8 Cross plots of δ^2H versus δ^{18}O of groundwater. The water samples are grouped according to their REY patterns

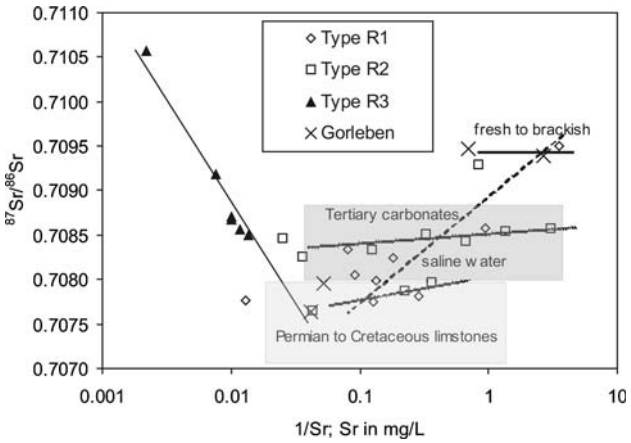

Fig. 9 Variation of Sr isotope ratios with 1/Sr in groundwater. Signature of samples refers to the defined R types. For details see text. Sr in mg/l. Arrays of Permian to Cretaceous limestones and Tertiary carbonates are taken from Veizer et al. (1999). Gorleben samples are taken from Kloppmann et al. (2001)

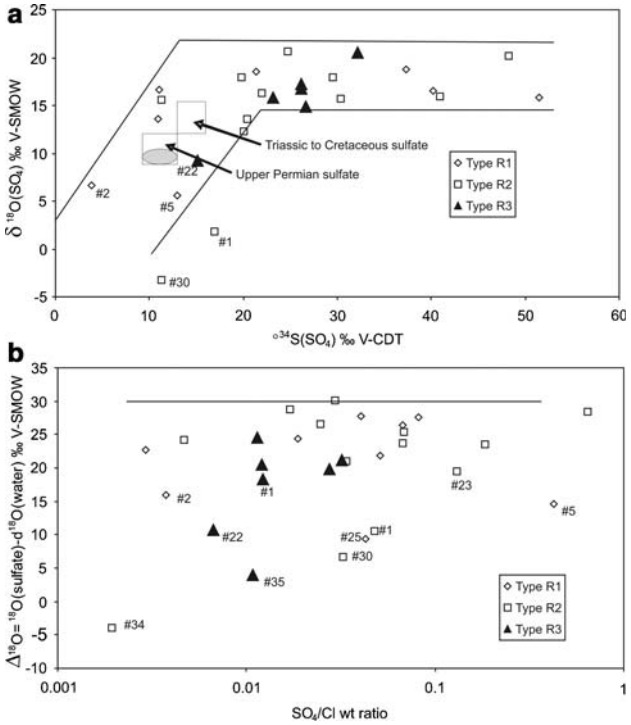

Fig. 10 Stable isotope of sulfate dissolved in groundwater. **a** $\delta^{18}O(SO_4^{2-})$ versus $\delta^{18}O(SO_4^{2-})$ and **b** $\Delta^{18}O = \delta^{18}O(SO_4^{2-}) - \delta^{18}O(H_2O)$ versus sulfate/chloride ratio. Signature of samples refers to R-types indicating the sources of water. $\Delta^{18}O$ of about 30‰ roughly corresponds to sulfate–water O-isotope exchange at about 15°C (Fritz et al. 1989). The *grey* field represents Gorleben Zechstein brines (Berner et al. 2002)

δ^{13}C(DIC)

δ^{13}C of dissolved inorganic carbon (DIC) varies from –3.7 to –22.7‰ (V-PDB) (Fig. 12). The range of –10 to –35‰ is typical for higher plants, algae and prokaryotes (Schidlowski et al. 1983). Most of the data are enclosed by DIC characterizing carbonate dissolution in closed and open systems. In Fig. 12a the samples #2 and #26 are outliers, which may be due to isotope exchange (Wigley et al. 1978). In this diagram mixing of different DIC sources should fall on straight lines. The only mixing line indicates mixing of water from a closed system with carbonate dissolution and from an open system in which sedimentary organic carbon (SOC, about –27‰) is oxidized. R1 and R2 type waters cover the whole field. R3 type waters show rather constant δ^{13}C values indicating limestone dissolution in a closed system (Fig. 12a) and show very similar HCO_3^-/Cl^- wt ratios (Fig. 12b).

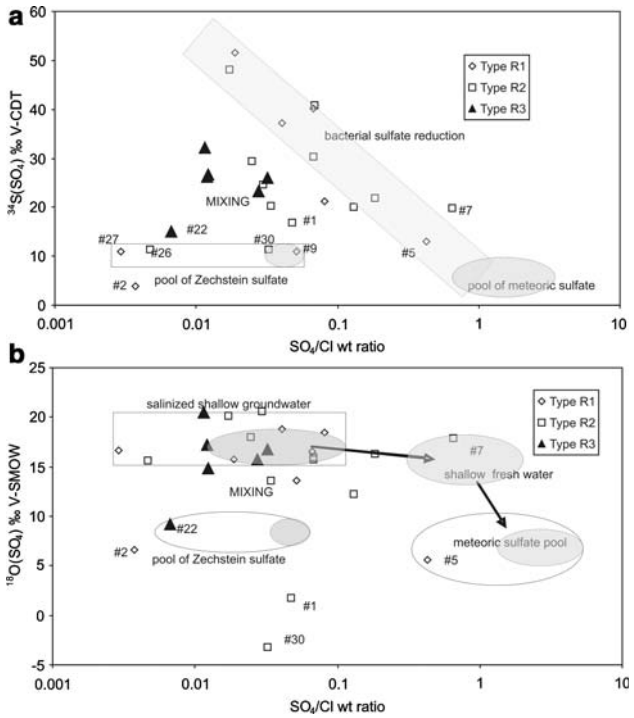

Fig. 11 Plot of $\delta^{34}S$ and $\delta^{18}O$ in sulphate as a function of SO_4/Cl wt ratio. The *grey* fields and their interpretations are taken from Berner et al. (2002). The *grey* field within the pool of Zechstein sulfate represents Gorleben samples

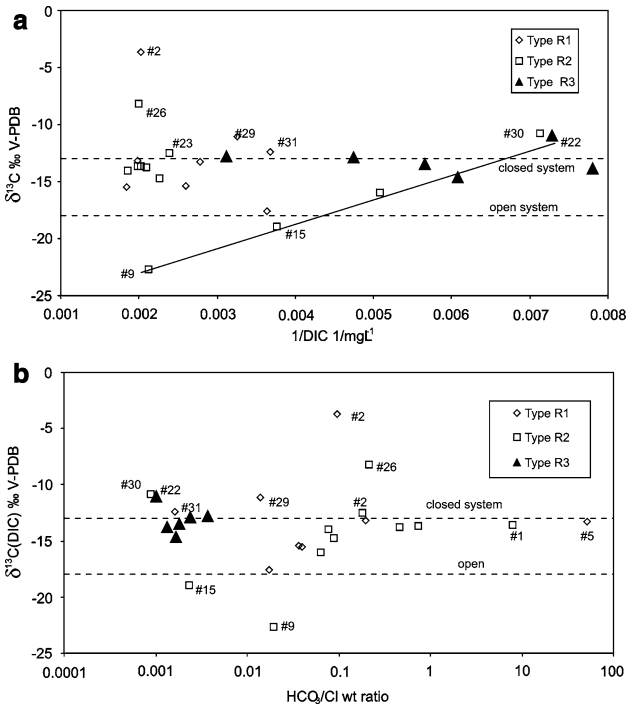

Fig. 12 Variation of $\delta^{13}C(DIC)$(with(1/DIC (**a**) and HCO_3^-/Cl^- (**b**). Grouping of groundwaters according to defined R types. Bacterial sulfate reduction leaves behind heavy sulfate but produces light CO_2. The *dashed lines* indicate calcite dissolution in closed and open systems based on 27‰ for mineralizing sedimentary organic carbon (Buckau et al. 2000)

Movement and salinization of groundwater

In view of depth, there is a clear separation of S1a + S1b and S2 + S3 type of water (Fig. 13a) and of R1 + R2 and R3 type (Fig. 13b). The weathering solution (type R1) and its equivalent type R2 after interaction with limestones dominantly occur in the upper 300 m (locally even at 2,000 m). The highly saline waters (mostly R3 type) reside below 1,000 m. Due to diapirism the geologic formations are strongly folded loosing any relationship to depth and highly saline waters even occur near the surface (Fig. 13). Although low-permeability layers are present, the distribution of R and S type waters is independent of geologic formations indicating either windows in aquicludes or their local to regional absence. This explains why type S1a water occurs at all depths in the study area and comprises half of the waters from the upper 300 m. The other half is shared by S1b, S2, S3 and S4 types. Out of these, S3 groundwater represents fresh water diluted by seawater from the Baltic Sea, which infiltrated because of over-exploitation of the freshwater system in the area of Lübeck. S4 type water represents dissolution of halite by infiltrating precipitation and S2 waters are derived from limestones or carbonate-rich boulder clays. The distinction between S1a and S1b depends on the amounts of dissolved evaporite minerals besides dissolved carbonates from limestones and on mixing with Ca–Cl brine. The S1 type of water demonstrates that dissolved Permian evaporites spread throughout the basin. Even the Rupelian clay (Lower Tertiary) is not impervious although this aquiclude is very important in separating the fresh water above from saline water below. Windows created by deep Pleistocene erosion channels facilitate exchange of water. Below the Rupelian, density-driven convection near diapirs may be the cause of up-coning saline waters (Magri et al. 2005).

Having in mind that S type patterns, $\delta^{34}S(SO_4)$ and $^{87}Sr^{86}/Sr$ ratios are linked to the source of solutes characterizing the groundwater, and R1 and R2 type waters show water isotopes (H and O) typical for Pleistocene precipitation, the distribution of these parameters evidence that water moves between geologic formations irrespective of low-permeability layers. Due to partial replacement of connate waters by younger ones and local dissolution of evaporites or mixing with older brines, the sampled evolved formations have little to do with the original one. Thus, none of the groundwaters represent connate water and the stratigraphic units of abstraction are not related to the source of water.

Spider diagrams show the presence of differently composed saline waters, which are either mixtures of precipitation and brines or the result of dissolution of evaporites

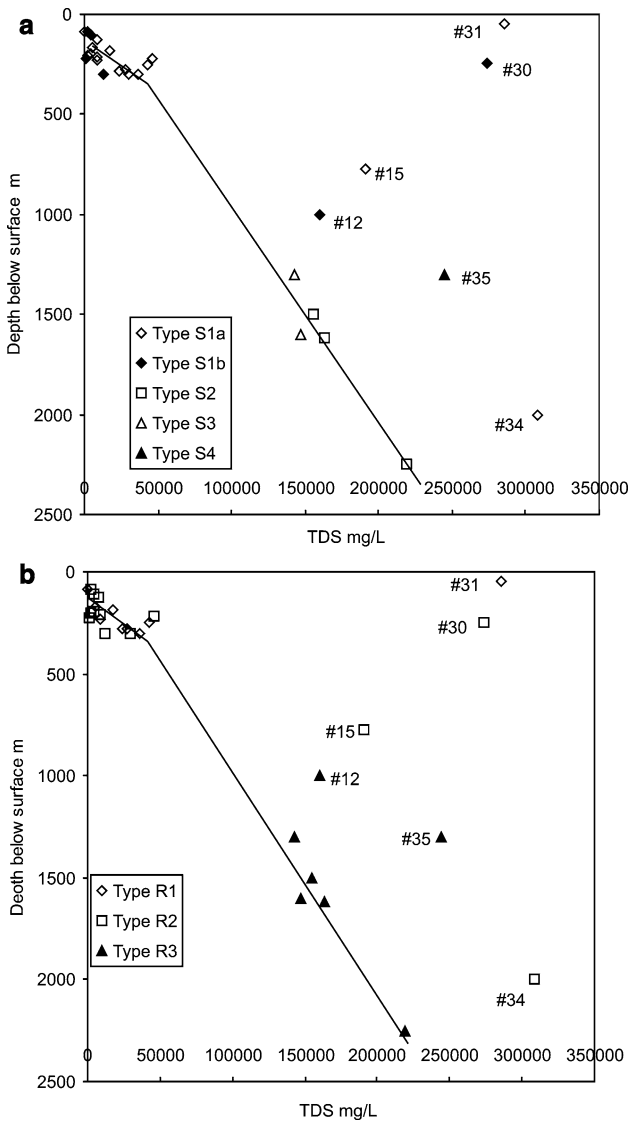

Fig. 13 Depth distribution of total dissolved salts in analysed samples. Samples are given by their spider patterns (**a**) and REY distribution patterns (**b**). Type R3 samples plot near the given line, whereas the spider patterns of the same samples are of S1b, S2, and S3. Although the chemical composition of the deep brines is variable (different S types) the REY patterns are very much the same. At about 300 m the gradient is changed. The samples #30, #31, #34, and #35 show occurrence of high-salinity waters at depths at which less saline waters prevail

(halite, sylvite, anhydrite) and/or carbonates. Marine evaporation brines may play a role in deep brines though no evidences for pure evaporation brines are found. Mixing of small amounts of brines with fresh water causes significant salinization but has only little influence on REY pattern and isotopic composition. Mixing of 10% of the deep brine with TDS of 300 g/l and infiltrating precipitation results in TDS of 30 g/l and in an increase of 3 and 0.4‰ in δ^2H and δ^{18}O, respectively.

The δ^2H of samples from the pre-Rupelian aquifer show some correlation with depth, however, with large scatter. Surprising is the fact that even samples from pre-Rupelian strata such as #7 (Upper Triassic) and #20 (Lower Triassic) are strongly influenced by Pleistocene water. Having in mind, that the Rupelian is considered as a low-permeability complex it should have prohibited exchange of water between the pre- and post-Rupelian aquifer complexes, if not interrupted or eroded by Pleistocene channels, which is definitely not the case at the sampling site of #7 in the Berlin area (Jortzig 2002). Therefore, lateral flow regimes have to be assumed because all pre-Rupelian aquifer systems to a depth of at least 500 m are isotopically characterized by Recent or Pleistocene recharge conditions.

Groundwater sample #8 (δ^{18}O = –9.85‰, δ^2H = –72.3‰), indicating Pleistocene precipitation conditions, belongs to the post-Rupelian Tertiary freshwater complex. Isotopic compositions of the post-Rupelian water are hydrodynamically plausible as no aquiclude separates the Quaternary and Upper Tertiary aquifers (Fig. 2). However, the salinization of #8 exceeding 5 g/l is not explicable without assuming contribution from underlying saline water bodies. At this locality lateral saline mass transport can be excluded because all neighboring observation wells of similar depth show fresh water and leachate of close-by salt diapirs does not protrude the Rupelian clay (Tesmer et al. 2007). Therefore, an ascending flow component must exist to cause salinization.

Apart from infiltration of Baltic seawater, subrosion of diapirs breaking through the Rupelian cause salinization of groundwater in the surroundings of Lübeck (#28, #25, #24), Lüneburg (#31) and Bad Bramstedt (#30) (Grube et al. 1996).

Conclusions

Considering major elements, REY distribution and isotopes conjointly, new insights into systematics of salinization in the North German Basin are achieved:

- The defined "R types" and "S types" of water assemble chemical data of water of seemingly the same origin but are in no way relatable to geologic formations in which these waters occur.
- S-type patterns, $\delta^{34}S(SO_4)$ and $^{87}Sr/^{86}Sr$ ratios describe the sources of solutes in groundwater. Solutes originate from interaction with soluble or reactive minerals along flow paths and in aquifer rocks, and from mixing with brines. R-type patterns and water isotopes (H and O) are linked to the catchment lithology, where mixing with deep-seated brines is minor.
- Pleistocene to Recent infiltration water (type R1) is salinized by mixing with high-salinity water dissolving

Permian to Jurassic evaporites resulting in S1, rarely S2 and S4 types of groundwater. In two cases local mixing with seawater is indicated by S3-type patterns. All these waters occur down to 800 m but mostly less than that.

- Deep thermo-saline waters (S1a and rarely S1b type patterns) represent dissolution of evaporites by a mixture of seawater or its evaporation brines (R3 type patterns) and precipitation ('heavy' water isotope ratios).
- All sulfates are of marine origin. $\delta^{34}S(SO_4)$ increases due to by bacterial reduction of sulfate.
- Sr isotopes reveal three sources of Sr: fast weathering of biotite (high Rb and Sr) and slow weathering of K-feldspar (high Rb, but low Sr) in the Pleistocene cover, and dissolution of limestones of Cretaceous to Permian age and Tertiary marls. Dissolution of limestones is the main source of Ca.
- The spider patterns demonstrate that none of the studied groundwaters are connate waters. Even the source of water in the deep brines is a mixture of seawater or its evaporation brines with precipitation. Some shallow saline waters are mixtures of seawater and precipitation.
- Although several low-permeability layers are present, saline waters enter the shallow post-Rupelian aquifer. It has to be concluded that dissolution brines of Permian and Triassic evaporites are incompletely sealed by their caprocks and further low-permeability layers.

Acknowledgments This study has been funded by the German Science Foundation (DFG) as part of SPP 1135 "Dynamics of sedimentary systems under varying stress conditions by example of the Central European Basin system". We thank B. Hansen, University of Göttingen, for supplying Sr isotope ratios. The authors appreciated the critical comments of W. Kloppmann and an anonymous reviewer who improved the manuscript.

References

Anders E, Grevesse N (1989) Abundance of elements: meteoric and solar. Geochim Cosmochim Acta 53:197–214

Bau M (1999) Scavenging of dissolved yttrium and rare earths by precipitating iron oxyhydroxide: experimental evidence for Ce oxidation, Y–Ho fractionation, and lanthanide tetrad effect. Geochim Cosmochim Acta 63:67–77

Bau M, Dulski P (1996) Anthropogenic origin of positive gadolinium anomalies in river waters. Earth Planet Sci Lett 143:245–255

Bausch WM (1968) Outlines of distribution of strontium in marine limestones. In: Müller G, Friedman GM (eds) Carbonate sedimentology in Central Europe. Springer, Berlin, pp 106–115

Bein A, Dutton AR (1993) Origin, distribution, and movement of brine in the Permian Basin (USA): a model for displacement of connate water. Geol Soc Am Bull 105:695–707

Bennett SS, Hanor JS (1987) Dynamics of subsurface salt dissolution at the Welsh Dome, Lousiana Gulf Coast. In: Lerch I, O'Brien JJ (eds) Dynamical geology of salt and related structures. Academic, Orlando, pp 653–677

Berner ZA, Stüben D, Leosson MA, Kling H (2002) S- and O isotopic character of dissolved sulphate in the cover rock aquifer of a Zechstein salt dome. Appl Geochem 17:1515–1528

Blum JD, Erel Y (1995) A silicate weathering mechanism linking increase in marine $^{87}Sr/^{86}Sr$ with global glaciation. Nature 373:415–418

Bruland KW, Lohan MC (2004) Controls of trace metals in seawater. In: Holland HD, Turekian KK (eds) Treatise on geochemistry, vol 6, pp 23–47. Elsevier, Amsterdam

Buckau G, Artinger R, Geyer S, Wolf M, Fritz P, Kim JI (2000) ^{14}C dating of Gorleben groundwater. Appl Geochem 15:583–597

Bullen TD, Kendall C (1998) Tracing of weathering reactions and water flowpaths: a multi-isotopic approach. In: Kendall C, McDonnel JJ (eds) Isotope tracers in catchment hydrology. Elsevier Amsterdam, pp 611–646

Carpenter AB (1978) Origin and chemical evolution of brines in sedimentary basins. Oklahoma Geol Surv Circ 79:60–77

Clark I, Fritz P (1997) Environmental isotopes in hydrogeology. Lewis Publishers, Boca Raton, pp 1–328

Claypool GE, Holser WT, Kaplan IR, Sakai H, Zak I (1980) The age curves of sulfur and oxygen isotopes in marine sulfate and their mutual interpretation. Chem Geol 28:199–260

Clayton RN, Friedmann I, Graf DL, Mayeda TK, Meents WF, Shimp NF (1966) The origin of saline formation waters. J Geophys Res 71:3869–3882

Craig H (1961) Isotopic variations in meteoric waters. Sci 133:1702–1703

Domenico PA, Robbins GA (1985) The displacement of connate water from aquifers. Geol Soc Am Bul 96:328–335

Dulski P (1994) Interferences of oxide, hydroxide and chloride analyte species in the determination of rare earth elements in geological samples by inductively coupled plasma-mass spectrometry. Fresenius J Anal Chem 350:194–203

Farber E, Vengosh A, Gavrieli I, Marie A, Bullen TD, Mayer B, Holtzman R, Segal M, Shavit U (2004) The origin and mechanism of salinization of the Lower Jordan River. Geochim Cosmochim Acta 60:1989–2006

Fontes JC, Matray JM (1993) Geochemistry and origin of formation brines from the Paris basin, France, 1: brines associated with Triassic salts. Chem Geol 109:149–175

Frape SK, Fritz P (1987) Geochemical trends for groundwaters from the Canadian shield. In: Fritz P, Frape SK (eds) Saline water and gases in crystalline rocks. Geol Ass Can Spec Pap 33:19–38

Fritz P, Basharmal GM, Drimmie RJ, Ibsen J, Quereshi RM (1989) Oxygen isotope exchange between sulphate and water during bacterial reduction of sulphate. Chem Geol 79:99–105

Giggenbach WF (1992) Isotopic shifts in waters from geothermal and volcanic systems along convergent plate boundaries and their origin. Earth Planet Sci Lett 113:495–510

Graf DL, Meents WF, Friedman I, Shimp NF (1966) The origin of saline formation waters III. Calcium–chloride waters. US Geol Surv Circ 397:1–60

Grube A, Lotz B (2004) Geological and numerical modeling of geogenic salinization in the area of the Lübeck basin (North Germany). Groundwater and saline intrusion. Selected papers from the 18th Salt Water Intrusion Meeting (SWIM), 31 May–3 June, Instituto geológico y minero de España, Cartagena, pp 183–195

Grube A, Nachtigall KH, Wichmann K (1996) Zur Grundwasserversalzung in Schleswig-Holstein. Meyniana 48:21–34

Grube A, Wichman K, Hahn J, Nachtigall KH (2000) Geogene Grundwasserversalzung in den Porengrundwasserleitern Norddeutschlands und ihre Bedeutung für die Wasserwirtschaft. Technologiezentrum Wasser Karlsruhe (TZW), Karlsruhe 9, pp 1–203

Hannemann M, Schirrmeister W (1998) Paläohydrogeologische Grundlagen der Entwicklung der Süß-/Salzwassergrenze und der Salzwasseraustritte in Brandenburg (Paleo-hydrogeological principles of the development of the fresh–/saltwater interface and the occurrence of saline springs in Brandenburg). Brandenburg Geowiss Beitr 5:61–72

Hanor JS (1994) Origin of saline fluids in sedimentary basins. In: Parnell J (ed) Geofluids: origin, migration and evolution of fluids in sedimentary basins. Geol Soc Spec Publ 151–178

Hardie LA (1990) The roles of rifting and hydrothermal $CaCl_2$ in the origin of potash evaporites—an hypothesis. Am J Sci 290:43–106

Herut B, Starinsky A, Katz A, Bein A (1990) The role of seawater freezing in the formation of subsurface brines. Geochim Cosmochim Acta 54:13–21

Jortzig H (2002) Verbreitung der Rupelfolge—Das Geopotenzial Brandenburgs. In: Stackebrandt W, Manhenke V (eds) Atlas zur Geologie von Brandenburg. Landesamt für Geowissenschaften und Rohstoffe Brandenburg, Kleinmachnow, vol 2, pp 72–73

Katz BG, Plummer LN, Busenberg E, Revesz KM, Jones BF, Lee TM (1995) Chemical evolution of groundwater near a sinkhole lake, northern Florida. 2. Chemical patterns, mass transfer modelling, and rates of mass transfer reactions. Water Resour Res 31:1565–1584

Kawabe I, Ohta A, Ishii S, Tokumura M, Miyauchi K (1999) REE partitioning between Fe–Mn oxyhydroxide precipitates and weakly acid NaCl solution: convex tetrad effect and fractionation of Y and Sc from heavy lanthanides. Geochem J 33:167–179

Kharaka YK, Berry FAF (1973) Simultaneous flow of water and solutes through geological membranes: I. experimental investigations. Geochim Cosmochim Acta 37:2577–2603

Klinge H, Vogel P, Schelkes K (1992) Chemical composition and origin of saline formation waters from the Konrad mine, Germany. Water rock interaction, Proceedings of the 7th international symposium on water–rock interaction/WRI-7, Park City, Utah, USA, 13–18 July, Balkema, Rotterdam pp 1117–1120

Kloppmann W, Negrel Ph, Casanova J, Klinge H, Schelke K, Guerrot C (2001) Halite dissolution derived brines in the vicinity of a Permian salt dome (N German Basin). Evidence from boron, strontium, oxygen and hydrogen isotopes. Geochim Cosmochim Acta 65:4087–4101

Knauth LP (1988) Origin and mixing history of brines, Palo Duro Basin, Texas, USA. Appl Geochem 3:455–474

Knöller K, Weise SM (in prep) Utilization of high temperature pyrolysis for the determination of $^{2}H/^{1}H$ and $^{18}O/^{16}O$ ratios in high salinity waters

Knöller K, Vogt C, Richnow H-H, Weise SM (2006) Sulfur and oxygen isotope fractionation during benzene, toluene, ethyl benzene, and xylene degradation by sulfate-reducing bacteria. Environ Sci Technol 40:3879–3885

Lerman A (1970) Chemical equilibrium and evolution of chloride brines. 50th Anniv Symp Miner Soc Spec Pap 3:291–306

Magri F, Bayer U, Jahnke C, Clausnitzer V, Diersch HJ, Fuhrmann J, Möller P, Pekdeger A, Tesmer M, Voigt H-J (2005) Fluid dynamics driven saline water in the North East German Basin. Int J Earth Sci 94:1056–1069

McLennan SM (1989) Rare earth elements in sedimentary rocks: influence of provenance and sedimentary processes. In: Lipin BR, McKray GA (eds) Geochemistry and mineralogy of rare earth elements. Mineralogical Society of America, Washington DC, pp 169–200

Metha S, Fryar AE, Banner JL (2000) Controls on the regional-scale salinization of the Ogallala aquifer, Southern High Plains, Texas USA. Appl Geochem 15:849–864

Mills AL (1988) Variation in $\delta^{13}C$ of stream bicarbonate: implications for sources of alkalinity. M.S. thesis, George Washington University, Washington DC, p 160

Möller P, Rosenthal E, Dulski P, Geyer S, Guttman Y (2003) Rare earths and yttrium hydrostratigraphy along the Lake Kinneret—Dead Sea—Arava transform fault, Israel. Appl Geochem 18:1613–1628

Möller P, Geyer S, Salameh E, Dulski P (2006a) Sources of mineralization of thermal groundwater of Jordan. Acta Hydrochim Hydrobiol 34:86–100

Möller P, Dulski P, Salameh E, Geyer S (2006b) Characterization of sources of thermal spring- and well water in Jordan by rare earth elements and yttrium distribution and stable isotopes of H_2O. Acta Hydrochim Hydrobiol 34:101–116

Möller P, Rosenthal E, Geyer S, Guttman J, Dulski P, Rybakov M, Zilberbrand M, Jahnke C, Flexer A (2007) Hydrochemical processes in the lower Jordan Valley and the Dead Sea area. Chem Geol 239:27–49

Nordstrom DK, Olsson T (1987) Fluid inclusions as a source of dissolved salts in deep granitic groundwaters. In: Fritz P, Frape SK (eds) Saline waters and gases in crystalline rocks. Geol Assoc Can Spec Pap 33:111–119

Quinn KA, Byrne RH, Schijf J (2004) Comparative scavenging of yttrium and the rare earth elements in seawater: competitive influences of solution and surface chemistry. Aquat Chem 100:59–80

Rosenthal E (1997) Thermosaline water of Ca–chloride composition: diagnostics and brine evolution. Environ Geol 32:245–249

Scheck M, Bayer U (1999) Evolution of the Northeast German Basin—inferences from a 3D structural model and subsidence analysis. Tectonophysics 313:145–168

Schidlowski M, Hayes JM, Kaplan IR (1983) Isotopic inferences of ancient biochemistries: carbon, sulphur, hydrogen and nitrogen. In: Schopf JW (ed) Earth's earliest biosphere: its origin and evolution. Princeton University Press, Princeton, pp 149–186

Sofer Z, Gat JR (1972) Activities and concentrations of oxygen-18 in concentrated aqueous salt solutions: analytical and geophysical implications. Earth Planet Sci Lett 15:232–238

Spencer DW (1987) Ocean chemistry—its central role in the evolution of the Earth. Chem Int 9/5:196–205

Starinsky A (1974) Relationship between Ca–chloride brines and sedimentary rocks in Isreal. Ph.D. thesis, Hebrew University, Jerusalem

Tesmer M, Otto R, Pekdeger A, Möller P, Bayer U, Magri F, Fuhrmann J, Enchery G, Jahnke C, Voigt H-J (2005) Migration paths and hydrochemical processes of groundwater salinization in different aquifer systems of the North German Basin. Terra Nostra 05/0:123–126

Tesmer M, Möller P, Wieland S, Jahnke C, Pekdeger A, Voigt H (2007) Deep reaching fluid flow in the North-East German Basin. Origin and processes of groundwater salinisation. Hydrol J, doi:10.1007/s10040-007-0176-y

Toran L, Harris RF (1989) Interpretation of sulfur and isotopes in biological and abiological sulphide oxidation. Geochim Coschim Acta 53:2341–2348

Van Stempvoort DR, Krouse HR (1994) Controls of $\delta^{18}O$ in sulphate—review of experimental data and applications to specific environments. In: Alpers CN, Blowes DW (eds) Environmental geochemistry of sulphide oxidation. Am Chem Soc Symp Ser 550:447–480

Veizer J, Ala D, Azmy K, Bruckschen P, Buhl D, Bruhn F, Carden GAF, Diener A, Ebneth S, Goddris Y, Jasper T, Korte C, Pawellek F, Podlaha OG, Strauss H (1999) $^{87}Sr/^{86}Sr$,($\delta^{13}C$ and $\delta^{18}O$ evolution of Phanerozoic seawater. Chem Geol 161:59–88

Wiegand B, Dietzel M, Bielert U, Groth P, Nansen BT (2001) 87Sr/86Sr-Verhältnisse als Tracer für geochemische Prozesse in

einem Lockergesteinsaquifer (Liebenau, NW Deutschland). Acta Hdrochim Hydrobiol 29:139–152

Wigley TML, Plummer LN, Pearson FJ (1978) Mass transfer and carbon isotope evolution in natural water systems. Geochim Cosmochim Acta 42:117–1139

Yanagisawa F, Sakai H (1983) Thermal decomposition of barium sulphate–vanadium pentaoxide–silica glass mixtures for preparation of sulfur dioxide in sulfur isotope ratio measurements. Anal Chem 55:985–987

Zieschang J (1974) Ergebnisse und Tendenzen hydrogeologischer Forschungen in der DDR (Results and tendencies of hydrogeological research in the GDR). Zt Angew Geol 20:452–458